Assessing the performance of near real-time rainfall products to represent spatiotemporal characteristics of extreme events

case study of a subtropical catchment in south-eastern Brazil

Laverde-Barajas, M.; Corzo Perez, G. A.; Dalfré Filho, J. G.; Solomatine, D. P.

DOI
10.1080/01431161.2018.1475773

Publication date
2018

Document Version
Final published version

Published in
International Journal of Remote Sensing

Citation (APA)
Laverde-Barajas, M., Corzo Perez, G. A., Dalfré Filho, J. G., & Solomatine, D. P. (2018). Assessing the performance of near real-time rainfall products to represent spatiotemporal characteristics of extreme events: case study of a subtropical catchment in south-eastern Brazil. *International Journal of Remote Sensing*, *39*(21), 7568-7586. https://doi.org/10.1080/01431161.2018.1475773

International Journal of Remote Sensing

ISSN: 0143-1161 (Print) 1366-5901 (Online) Journal homepage: https://www.tandfonline.com/loi/tres20

Assessing the performance of near real-time rainfall products to represent spatiotemporal characteristics of extreme events: case study of a subtropical catchment in south-eastern Brazil

M. Laverde-Barajas, G.A. Corzo Perez, J.G. Dalfré Filho & D.P Solomatine

To cite this article: M. Laverde-Barajas, G.A. Corzo Perez, J.G. Dalfré Filho & D.P Solomatine (2018) Assessing the performance of near real-time rainfall products to represent spatiotemporal characteristics of extreme events: case study of a subtropical catchment in south-eastern Brazil, International Journal of Remote Sensing, 39:21, 7568-7586, DOI: 10.1080/01431161.2018.1475773

To link to this article: https://doi.org/10.1080/01431161.2018.1475773

INTERNATIONAL JOURNAL OF REMOTE SENSING
2018, VOL. 39, NO. 21, 7568–7586
https://doi.org/10.1080/01431161.2018.1475773

Taylor & Francis
Taylor & Francis Group

Assessing the performance of near real-time rainfall products to represent spatiotemporal characteristics of extreme events: case study of a subtropical catchment in south-eastern Brazil

M. Laverde-Barajas [a,b], G.A. Corzo Perez [a], J.G. Dalfré Filho [c] and D. P Solomatine [a,b]

[a]Integrated Water Systems and Governance department, IHE Delft Institute for Water Education, Delft, The Netherlands; [b]Water Resources Section, Delft University of Technology, Delft, The Netherlands; [c]School of Civil Engineering, Architecture and Urbanism, University of Campinas, UNICAMP, Campinas, Brazil

ABSTRACT

This study evaluates the performance of four Near Real-Time (NRT) satellite rainfall products in estimating the spatiotemporal characteristics of different extreme rainfall events in a subtropical catchment in south-eastern Brazil. The Climate Prediction Centre Morphing algorithm (CMORPH), Tropical Rainfall Measuring Mission, Multisatellite Precipitation Analysis in real time (TMPA-RT), the Precipitation Estimation from Remotely Sensed Information using Artificial Neural Networks-Global Cloud Classification System (PERSIANN-GCCS), and the Hydro-Estimator are evaluated for monsoon seasons, based on their capability to represent four types of rainfall events distinguished for: (1) local and short duration, (2) long-lasting event, (3) short and spatial extent, and (4) spatial extent and long lasting. Since the events are defined relative to a percentile, the relative performance variation at different threshold levels (75th, 90th, and 95th) is also evaluated. The data from the 13 Automatic Weather Stations (AWSs) for the period from 2007 to 2014 are used as the reference. The results show that the product performance highly depends on the spatiotemporal characteristics of rainfall events. All four products tend to overestimate intense rainfall in the study area, especially in high altitude zones. CMORPH had the best overall performance to estimate different types of extreme spatiotemporal events. The results allow for developing a better understanding of the accuracy of the NRT products for the estimation of different types of rainfall events.

ARTICLE HISTORY
Received 11 April 2017
Accepted 1 May 2018

1. Introduction

The distribution and intensity of extreme rainfall play an important role in the hydrological cycle. The characteristics of rainfall events such as the magnitude, duration, and spatial extent determine the level of damage associated with natural hazards. In this context, an accurate representation of the temporal and spatial components of extreme

CONTACT M. Laverde-Barajas m.laverde@un-ihe.org IHE Delft Institute for Water Education, The Netherlands

rainfall is crucial for the correct assessment of water-resource availability and prediction of potential water-related risks (Thiemig et al. 2012).

A wide range of rainfall measurement devices and systems are available, such as rain gauges, weather radars, and meteorological satellites. Rainfall gauges are traditionally used for providing accurate rainfall measurements. However, in many regions, this information is often scarce, discontinuous, and is not enough to capture the spatiotemporal variability of rainfall (Michaelides et al. 2009; Kidd et al. 2016). Additionally, measurements are subject to systematic errors as a consequence of human interference and problems in the instruments, among others. Alternatively, weather radars estimate rainfall over large areas with a spatial resolution as lower as 1 km^2 every 5 or 10 min. Despite the detailed description of rainfall, weather radars are very expensive to install and are associated with several sources of uncertainty due to errors in the reflectivity–rain rate (Z–R) relationship, signal attenuation, or contamination (Villarini, Serinaldi, and Krajewski 2008; Hasan et al. 2014; Peleg, Ben-Asher, and Morin 2013).

During the last two–three decades, earth observation systems have been providing an important input to the weather monitoring and forecasting systems (e.g. Kidd et al. 2009; Pan, Li, and Wood 2010; Azarderakhsh et al. 2011). Satellite-based rainfall products provide uninterrupted global information with an up to 0.5 h interval and up to 8 km spatial resolution. There are many operational high-resolution satellite precipitation products available for download on the Internet (e.g. Huffman et al. 2007; Joyce et al. 2004; Sorooshian et al. 2000). These products employ multiple algorithms to data from passive microwave (PMW) and infrared (IR) sensors. IR sensors assess the rainfall via the cloud-top temperature, while PMW sensors analyse emission, absorption, and diffusion signals inside the cloud. The combination of those operational instruments has allowed for a greater accuracy in rainfall estimation (Huffman et al. 2007). Despite the multiple advantages of satellite-based products, several studies have shown errors in satellite rainfall estimations related to the measuring devices (e.g. Hu et al. 2016; Qiao et al. 2014), the size of the basin (e.g. Moazami et al. 2013), the climate regimes and seasons (e.g. Thiemig et al. 2012; Sapiano and Arkin 2009; Mei et al. 2014), and the geographical conditions (e.g. Mei et al. 2015; Dinku et al. 2007; Guo et al. 2015; AghaKouchak et al. 2011). For extreme rainfall detection, uncertainties associated with the capacity of detecting the heavy rainfall rate at short temporal resolutions (e.g. AghaKouchak et al. 2011; Marra et al. 2017) have limited their use in operational applications.

Several studies have evaluated the behaviour of satellite-based products to represent the spatial and temporal characteristics of extreme events. Temporal capabilities of different NRT satellite products have been investigated by Mehran and Amir (2014) across the United States. Analysing heavy rainfall at different temporal accumulations, the authors indicated that all high-temporal resolution products (3-hourly) presented problems for estimating high rainfall rates. Gebregiorgis and Hossain (2015) analysed the spatial performance of different NRT products around the world. Based on error variance models, they showed how diverse geophysical settings impact the products' performance. In the case of South America, just a few studies have analysed the performance of satellite-based rainfall products in estimating the spatiotemporal characteristics of extreme rainfall. Ringard et al. (2015) evaluated four satellite-based rainfall products against *in situ* measurements over French Guiana and North Brazil. Dividing the study area into six climatic zones and analysing daily and monthly rainfall data, their analysis

showed that estimates of low-intensity rainfall have relatively high accuracy, while convective-type rainfalls were poorly estimated by satellite products. Boers et al. (2013) analysed the spatial characteristics of extreme events estimated by two satellite-based products and one re-analysis data set over the South American monsoon system. Using the complex networks theory, these researchers found substantial differences in estimating the extreme rainfall patterns between the different rainfall products, especially in the southeast of Brazil.

For hydrological applications, rainfall analysis needs a better understanding of how the characteristics of an extreme event (intensity, duration, and spatial distribution) are represented by different data sets. The main objective of this study is to evaluate the performance of the four near real-time (NRT) satellite-based rainfall products to represent different extreme rainfall events (EREs). The raw version of Climate Prediction Centre (CPC) Morphing algorithm (CMORPH; Joyce et al. 2004), the Tropical Rainfall Measuring Mission, Multisatellite Precipitation Analysis in Real Time (TMPA-RT; Huffman et al. 2010; Huffman et al. 2007), the Precipitation Estimation from Remotely Sensed Information using Artificial Neural Networks-Global Cloud Classification System (PERSIANN-GCCS; Sorooshian et al. 2000) version 7, and the Hydro-Estimator (Hydro; Scofield and Kuligowski 2003) are compared against an Automatic Weather Station network (AWS; CIIAGRO, 2017) during the core of monsoon seasons (December, January, and February) from 2007 to 2014. The spatiotemporal analysis focuses on the four different extreme event types proposed by Boers et al. (2015).

2. Study area

We are considering the subtropical catchments of the Piracicaba, Capivari, and Jundiai rivers located at the southeast of Brazil (PCJ) (Figure 1). The PCJ covers a drainage area of 14,138 km^2 with an elevation ranging from 436 to 2074 AMSL distributed in three zones: upper altitude zones, located on the east side and in a small area near to Corumbataí; intermediate or middle altitude zones, mainly located in the central part; and low altitude zones, located in the western part, where the rivers flow to Tietê River. The average rainfall ranges between 1300 and 1500 mm per year.

This area is strongly impacted by inter- and extra-tropical climatic conditions, such as the convective precipitation band of the South Atlantic Convergence Zone, one of the most distinctive features of the South American Monsoon System (Boers et al. 2013). This factor makes the area prone to extreme landslides and flash floods (Sprissler 2011). During the period of 2000 to 2011, natural hazards related to heavy rainfall affected more than 26,000 habitants in the PCJ catchments. In this research, we analysed the climatic conditions during the core of monsoon in South America from December to February, between the years of 2007 and 2014.

3. Rainfall products

The four NRT satellite-based rainfall products are evaluated in seven monsoon seasons from a common analysis period from December 2007 to February 2014. This selection is based on the following criteria: (1) a good correlation in previous studies over the region; (2) good spatial and temporal resolution; (3) operation in NRT or 'early run'

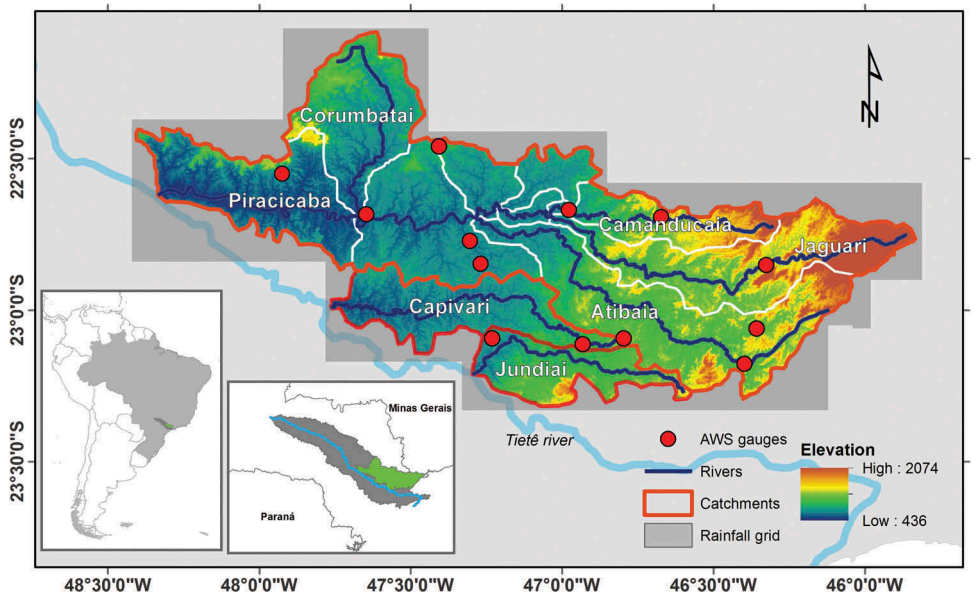

Figure 1. Elevation map and AWS network (red dots) for the catchment of Piracicaba, Capivari, and Jundiai rivers. The Shuttle Radar Topography Mission (SRTM) Version 3.0 is available at https://earthdata.nasa.gov. Catchment areas and river network are available at http://www.ana.gov.br.

satellite products. It is to be highlighted that the NRT products are referred to non-gauge corrected rainfall estimations, which are available soon after their generation; (4) common covering period over the monsoon seasons; and (5) their free access and publication. The latency of these rainfall products ranges from 1 to 18 h. Within the products evaluated, two products combine passive microwave and infrared sensors (IR-PMW) and two use infrared sensors to estimate rainfall (IR)(Table 1).

Since each product has different spatial and temporal resolutions, rainfall products with spatial resolution finer than 0.25° were scaled up by aggregation in which the products are averaged to larger scales for matching the spatial resolution of the referenced data set. Note that assumptions used in the aggregation algorithm and the whole nature of aggregation bring uncertainties as well. Aggregated rainfall data have their own contribution to the total error (Gebere et al. 2015), however, in this article, they are not taken into account.

The following section gives a brief description of the four NRT satellite-based rainfall products.

3.1. *CPC MORPHING (*CMORPH)

The CPC MORPHING product (CMORPH) was developed by the NOAA Climate Prediction Centre to integrate the main advantages of passive microwave (high quality) and infrared sensors (Joyce et al. 2004). CMORPH combines the data from the sensors in two stages. First, the atmospheric motion vectors from two successive IR images are generated every 30 min. Second, the generated motion vectors are used to propagate the rainfall fields from diverse

microwave data. CMORPH is available at 8 km (0.0727°) spatial resolution with 3 h temporal resolution. This study uses the CMORPH Version 1.0 Raw at 0.25° spatial resolution with 3 h temporal resolution.

3.2. *TMPA-RT (3B42V7)*

TRMM Multisatellite Precipitation Analysis (TMPA) Version 7 is a rainfall estimation product from the TRMM NASA mission. In this real-time version, TMPA combines different passive microwave and infrared sensors to measure rainfall in the tropical and subtropical regions around the world. The passive microwave sensors used include the Microwave Imager (TMI), the Special Sensor Microwave Imager/Sounder (SSMIS), the Advanced Microwaved Scanning Radiometer (AMSR-E), the Advanced Microwave Sounding Unit (AMSU), and the Microwave Humidity Sounder (MHS). Infrared measurements are obtained from GOES, Meteosat 5 and 7 geostationary meteorological satellites (GMSs), and NOAA-12 geostationary satellites.

The real-time TMPA (TMPA-RT) is conducted within 6–9 h of the measurement. Huffman et al. (2010) presented a detailed description of the processing and the generation of TMPA-RT. It had three major updates during the last decade (versions 5, 6, and 7 (see Yong et al. 2010; Yong et al. 2012)). One of the important upgrades included in the TMPA-RT is the Climatological Calibration Algorithm (CCA). This algorithm uses climatological gauge information, to reduce the systematic biases of the estimation, maintaining the near real-time availability (Yong et al. 2014). TMPA-RT is available since January 1998, at 0.25° spatial resolution, 3 hourly temporal resolution, and with a 50°N–50°S spatial coverage.

3.3. *PERSIANN-GCCS*

PERSIANN is an algorithm based on a classification procedure using an artificial neural network (ANN). The input data of PERSIANN are the brightness temperature measurements obtained from IR sensors of the NOAA's Geostationary Operational Environmental Satellite (GOES) and Meteosat 5 and 7 geostationary meteorological satellites (GMSs). The TMI from TRMM is used as a learning value for training the ANN, which adjusts the IR-derived rainfall rates to represent the behaviour of the derived TMI. This method allows for a fast estimation of rainfall at 0.04° each half hour. In this research, we used the PERSIANN with the Global Cloud Classification System at 3 hourly temporal duration and the spatial resolution scaled up by aggregation from 0.04° to 0.25°.

4. Hydro-Estimator

The Hydro is based on the automatic precipitation estimation algorithm NESDIS (Vicente, Scofield, and Paul Menzel 1998). Similar to PERSIANN, Hydro uses the infrared cloud-top brightness temperature information from GOES as primary information to estimate rainfall rates. In addition, Hydro uses atmospheric information modelled from the Global Forecast System (GFS) to correct the rainfall rate estimations for non-detected factors in the satellite sensor such as moisture availability, evaporation, orographic modulation, and thermodynamic profile effects. This product has been widely used as

the main input in many flash flood early warning systems around the world, including the CAFFG System in Central America, ALERT in the United States, Argentina, Australia, China, and India among others and the TerraMA2 in Brazil. Hydro is available since 2003 (for the United States only), and global estimations are available since 2007. In this research, the spatial resolution of Hydro was scaled up by aggregation from 0.04° to 0.25° and the temporal resolution from 15 min to 3 h.

4.1. *Reference data*

Ground truth data are based on 13 Automatic Weather Station (AWS) observations provided by the Integrated Centre of Agrometeorological information CIIAGRO (CIIAGRO, Centro Integrado de Informações Agrometeorológicas 2017) (Figure 1). These stations are part of a dense network of hourly real-time information for agrometeorological monitoring in the PCJ catchment. The data were quality controlled to reduce possible errors and noise in the measurements. In the first part, we compared the product at the point-based location scale to avoid taking interpolation errors into account. However, in the following parts, we used interpolated gridded data to represent the spatial representation of the referenced data. Hourly AWS measurements were interpolated using the Inverse Distance Weighed method (IDW) (Wackernagel 2003) set to 0.25° × 0.25°from 2007 to 2014.

5. Methodology

The methodology involves three parts: First, we analyse the spatial error distribution at different high intensity levels between satellite-based rainfall products and AWS gauges during monsoon seasons. In the second part, we evaluate the performance of the products to identify different extreme rainfall event (ERE) types. In the third part, we assess the sensitivity of the event-based performance to different intensity rainfall thresholds.

5.1. *Error distribution of satellite products at high-intensity rainfall levels*

The spatial error of satellite products is analysed on a point-cell basis for the three intervals: above the 75th percentile (strong rainfall), above the 90th percentile (extreme rainfall), and above the 95th percentile (most extreme rainfall). This method compares the grid points of satellite products and the reference data with the nearest rain gauge values (Thiemig et al. 2012; Dembélé and Zwart 2016). However, in the areas where two or more stations lie in a cell, rainfall values are compared using the average-point measurements to the cell (Thiemig et al. 2012). In these cases, the spatial rainfall variability will be limited by the product resolution which may lead to an under or overestimation (Peleg et al. 2016). For this analysis, we used three widely used statistical measures to quantify the errors: the correlation coefficient (r) to analyse the linear correlation between the satellite products and AWS measurements, the root mean square error (RMSE) to evaluate the magnitude error, and the relative bias (Bias) to evaluate the systematic bias of the products (Li, Zhang, and Xu 2014) (equations 1–3).

$$r = \frac{\sum_{i=1}^{n}(P_{\text{sat}_i} - \bar{P}_{\text{sat}}) \times (P_{\text{ref}_i} - \bar{P}_{\text{ref}})}{\sqrt{\sum_{i=1}^{n}(P_{\text{sat}_i} - \bar{P}_{\text{sat}})^2} \times \sqrt{\sum_{i=1}^{n}(P_{\text{ref}_i} - \bar{P}_{\text{ref}})^2}}, \tag{1}$$

$$\text{RMSE} = \sqrt{\frac{1}{n}\sum_{i=1}^{n}(P_{\text{sat}_i} - P_{\text{ref}_i})^2}, \tag{2}$$

$$\text{Bias} = \frac{\sum_{i=1}^{n} P_{\text{sat}_i} - P_{\text{ref}_i}}{\sum_{i=1}^{n} P_{\text{ref}_i}} \times 100, \tag{3}$$

where n is the number of samples; P_{sat} are the satellite-based measurements and P_{ref} is the reference value, and $\bar{P}_{\text{sat}}\bar{P}_{\text{ref}}$ are the mean of the satellite measurements and the reference values.

5.2. *Performance in detecting different EREs in spatiotemporal context*

The performance of NRT products to represent rainfall events is evaluated considering temporal and spatial characteristics. For intense rainfall considered as extreme (above the 90th percentile), we defined different ERE types according to the classification proposed by Boers et al. (2015). This methodology defines four types of rainfall events defined by their duration and spatial extension:

(a) Local and short extreme (LSE) events, which are only determined by their high magnitude.
(b) Local and long-lasting extreme (LLE) events, which are characterized by long duration and high magnitude.
(c) Spatially extensive extreme (SEE) events, which are identified by their extension and high magnitude. In this study, unlike proposed by Boers et al. (Boers et al. 2015), SEE is composed of events (connected) with a high magnitude. This was done to analyse the spatiotemporal behaviour at the same threshold.
(d) Spatially extensive and long-lasting extreme (SLE) events, which are determined by their high magnitude, long duration, and wide extension.

To identify the classes of EREs the following procedure is used:

(1) Estimate the temporal duration of each event, by employing a running-mean filter to the gridded rainfall time series P at time step i:

$$\tilde{P}_i = \frac{\sum_{s=-w}^{w} P_{i-s}}{2w+1}, \tag{4}$$

Table 1. NRT satellite-based rainfall products used.

Product	Provider	Spatial coverage	Temporal coverage	Type	Spatial and temp res.
CMORPH V1.0 Raw	NOAA-CPC (NOAA 2002a)	60°N–60°S	Since 1 January 1998	IR-PMW	0.07°approx./3 h
TMPA-RT	NASA/JAXA (NASA 2000)	50°N–50°S	Since 1 January 1998	IR-PMW	0.25°/3 h
PERSIANN-GCCS	UC Irvine (UC Irvine 2003)	60°N–60°S	Since 1 March 2000	IR	0.04° approx./0.5 h
Hydro-Estimator	NOAA/NESDIS (NOAA 2002b)	90°N–90°S	Since 1 January 2007	IR	0.04°/15 min

where P_i is the filter input and $\tilde{P}_i$ is the filtered rainfall value. This method uses the moving average period defined as $2w + 1$. w is the width of the running-mean filter given by Table 2.

(2) Considering P_i and $\tilde{P}_i$ to be samples of rainfall intensities, compute the pth percentile of these samples (for rainfall above 0.2 mm). Rainfall events are defined as time steps i for which P_i and $\tilde{P}_i$ are above a threshold T^p, depending on the type of event (strong, extreme, and most extreme) (Table 2).

$$e_i := \begin{cases} 1, \text{if} P_i | \tilde{P}_i > T^p, \\ 0, \text{otherwise} \end{cases}, \tag{5}$$

where e_i is a binary event indicator associated with the time step i. T^p is the threshold corresponding to the pth percentile.

(3) To identify the spatial extent of an extreme rainfall, we employed the so-called connected component labelling method to group similar rain cells into homogeneous groups (Szeliski 2010; He et al. 2017). This method connects cell values identified as an event in each time step as object pixels. This spatial type of event e_i^q is defined by the size of its connected label relative to the spatial threshold S_i^q (Boers et al. 2015).

$$\begin{cases} e_i^q := \begin{cases} 1, \text{ if} C_i^q > S^q, \\ 0, \text{otherwise} \end{cases}, \end{cases} \tag{6}$$

where C_i^q is the group of connected cells (considered as events) at each time step and q is the spatial threshold in space. Considering the hydro-meteorological scales of rainfall systems observed in the region, we defined extensive events as events with an area bigger than 2° × 2° (S_i^q= 8 cells; each of 0.25° × 0.25°).

Taking into account the characteristics of ERE, we defined the spatial and temporal component of each ERE type. Table 2 shows the components of each type of ERE. It should be noted that these four classes are not mutually exclusive, so one event may be classified into two or more types of ERE.

Considering the magnitude, duration, and spatial extension of the reference data set during monsoon seasons, we analysed the frequency and spatial patterns for all types of ERE. To avoid double counting of EREs, we separated joint EREs selecting the inter-arrival time of each type of event (e.g. Dunkerley 2008; Dunkerley 2010). By concept, LSE and SEE events usually range between 3 and 6 h, while LLE lasts for 9–15 h and the SLE event ranges from 6 to 12 h.

Table 2. Spatial and temporal characteristics of each ERE type.

ERE type	Magnitude	Temporal (w)	Spatial (q)
LSE	T^{75}, T^{90}, T^{95}	-	-
LLE	T^{75}, T^{90}, T^{95}	2	-
SEE	T^{75}, T^{90}, T^{95}	-	8 cells
SLE	T^{75}, T^{90}, T^{95}	2	8 cells

The capabilities of the NRT satellite-based rainfall products for each ERE type are evaluated based on four skill score metrics proposed by AghaKouchak and Mehran (2013) and Wilks (2011). The Frequency Bias Index, Probability of Detection, False alarm ratio, and Critical Success Index are used to evaluate the performance in relation to rainfall events, as presented in equations 7–10:

(a) The Event-based Frequency Bias Index (EFBI) indicates the level of underestimation or overestimation of an event 'e'. It ranges from 0 to infinity with the perfect score of 1. I represents the indicator function and n represents the number exceedances

$$\mathrm{EFBI} = \frac{\sum_{i=1}^{n} I(P_{\mathrm{sat}_i} | P_{\mathrm{sat}_i} \in \mathrm{e} \& P_{\mathrm{ref}_i} \notin \mathrm{e}) + \sum_{i=1}^{n} I(P_{\mathrm{sat}_i} | P_{\mathrm{sat}_i} \notin e \& P_{\mathrm{ref}_i} \in \mathrm{e})}{\sum_{i=1}^{n} I(P_{\mathrm{sat}_i} | P_{\mathrm{sat}_i} \in \mathrm{e} \& P_{\mathrm{ref}_i} \in \mathrm{e}) + \sum_{i=1}^{n} I(P_{\mathrm{ref}_i} | P_{\mathrm{sat}_i} \in \mathrm{e} \& P_{\mathrm{ref}_i} \notin \mathrm{e})} \tag{7}$$

(b) Event-based Probability of Detection (EPOD) is defined as the ratio of the correct detections of an event 'e.' It ranges from 0 to 1, with the perfect score of 1.

$$\mathrm{EPOD} = \frac{\sum_{i=1}^{n} I(P_{\mathrm{sat}_i} | P_{\mathrm{sat}_i} \in \mathrm{e} \& P_{\mathrm{ref}_i} \in \mathrm{e})}{\sum_{i=1}^{n} I(P_{\mathrm{sat}_i} | P_{\mathrm{sat}_i} \in \mathrm{e} \& P_{\mathrm{ref}_i} \in \mathrm{e}) + \sum_{i=1}^{n} I(P_{\mathrm{sat}_i} | P_{\mathrm{sat}_i} \notin \mathrm{e} \& P_{\mathrm{ref}_i} \in \mathrm{e})} \tag{8}$$

(c) The Event-based False alarm ratio (EFAR) represents the ratio of the incorrect detections belonging to the event 'e.' It ranges from 0 to 1 with the perfect score of 0.

$$\mathrm{EFAR} = \frac{\sum_{i=1}^{n} I(P_{\mathrm{sat}_i} | P_{\mathrm{sat}_i} \in \mathrm{e} \& P_{\mathrm{ref}_i} \notin \mathrm{e})}{\sum_{i=1}^{n} I(P_{\mathrm{sat}_i} | P_{\mathrm{sat}_i} \in \mathrm{e} \& P_{\mathrm{ref}_i} \in \mathrm{e}) + \sum_{i=1}^{n} I(P_{\mathrm{ref}_i} | P_{\mathrm{sat}_i} \in \mathrm{e} \& P_{\mathrm{ref}_i} \notin \mathrm{e})} \tag{9}$$

(d) The Event-based Critical Success Index (ECSI) corresponds to the combination of EPOD and EFAR to identify the overall performance skill of ERE. It ranges from 0 to 1, with 0 as the perfect score

$$\mathrm{ECSI} = \frac{\sum_{i=1}^{n} I(P_{\mathrm{sat}_i} | P_{\mathrm{sat}_i} \in \mathrm{e} \& P_{\mathrm{ref}_i} \in \mathrm{e})}{\sum_{i=1}^{n} I(P_{\mathrm{sat}_i} | P_{\mathrm{sat}_i} \in \mathrm{e} \& P_{\mathrm{ref}_i} \in \mathrm{e}) + I(P_{\mathrm{ref}_i} | P_{\mathrm{sat}_i} \notin \mathrm{e} \& P_{\mathrm{ref}_i} > \mathrm{e}) + I(P_{\mathrm{sat}_i} | P_{\mathrm{sat}_i} \in \mathrm{e} \& P_{\mathrm{ref}_i} \notin \mathrm{e})} \tag{10}$$

5.3. *Event-based performance for different rainfall intensities*

The sensitivity of the event-based performance at different intensity rainfall thresholds is evaluated in the third part of the methodology. Following the process described in section 4.2, we compared the products' performances for rainfall events defined above T^{75}, T^{90}, and T^{95} percentiles. For each satellite product, the performance is evaluated using EFBI, EPOD, EFAR, and ECSI scores.

6. Results and discussion

6.1. *Error distribution of satellite products at high intensity levels*

Figure 2 shows the spatial location of errors of the satellite products, compared to the reference AWS data during monsoon seasons from 2007 to 2014. Figure 2(a–**c)** present the spatial distribution of *r*, RMSE, and Bias, and Figure 2(d) shows the cross-correlation between the satellite products and the reference data over the study area. According to the results, the satellite products had problems for the high altitude zones. CMORPH was the product with the lowest quantitative errors, indicated by the highest correlation (mean *r* 0.65), and the lowest magnitude error and the systematic bias (mean RMSE 0.58 mm h^{-1}, Bias 4.5%). For TMPA-RT and PERSIANN-GCCS, errors were generally high for elevated altitude zones. TMPA-RT presented a better correlation and lower Bias than PERSIANN-GCCS, however, the error magnitude was higher. Hydro was the product with the highest error over the whole study area with *r* and RMSE values of around 0.33 and 1.16 mm h^{-1}, respectively, and a Bias higher than 40%.

Concerning the error measurement at different rainfall levels, Figure 3 shows the *r*, RMSE, and Bias errors of NRT products above 75th, 90th, and 95th percentile thresholds: error increases with an increase in rainfall intensity. CMORPH and TMPA-RT had the lowest errors at high intensities. CMORPH presented the highest correlation coefficient dropping from 0.4 at T^{75} to 0.2 at T^{95}, while TMPA-RT had the lowest overestimation increasing from 25% at T^{75} to 38% at T^{95}. In contrast, PERSIANN-GCCS and Hydro have the highest errors (the lowest correlation and high overestimation).

6.2. *Performance of satellite-based products to represent different types of ERE*

6.2.1. *Local and short extreme (LSE) events*

The performance of satellite-based products in terms of EFBI, EPOD, EFAR, and ECSI for LSEs is shown in Figure 4. In general, performance is not very high, especially at high altitude zones. CMORPH showed better performance (low EFBI and EFAR). TMPA-RT showed the best EPOD and together with CMORPH had the better ESCI score distributed

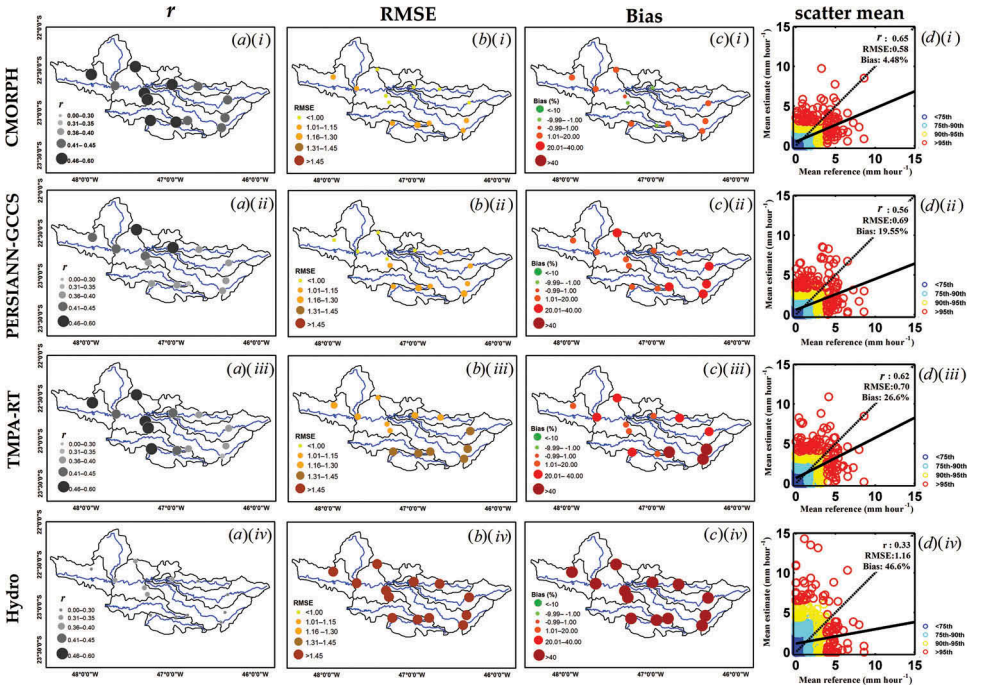

Figure 2. Spatial distribution of (a) *r*; (b) RMSE; (c) Bias errors; and (d) scatterplot of the mean rainfall of (i) CMORPH, (ii) PERSIANN-GCCS, (iii) TMPA-RT, (iv) Hydro, during monsoon seasons from 2007 to 2014.

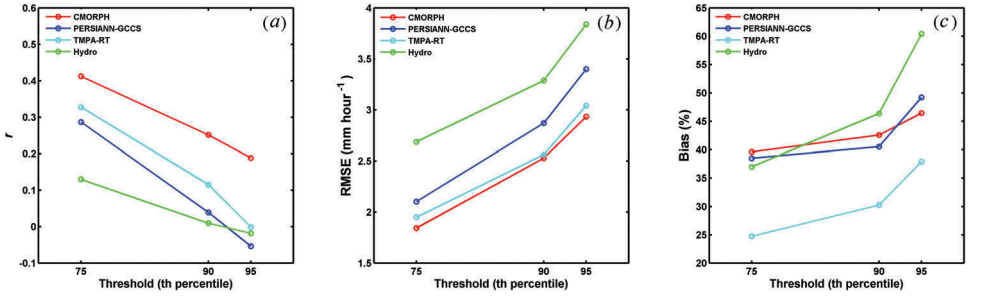

Figure 3. Quantitative errors of satellite rainfall products versus AWS measurements above different rainfall thresholds. (a) *r*; (b) RMSE; and (c) Bias.

mainly in the middle and low altitude zones. PERSIANN-GCCS and Hydro had a poor score for LSE detection, being the products with the lowest performance for LSEs.

6.2.2. *Local and long-lasting extreme (LLE) events*

Figure 5 presents the performance of satellite products for LLE events. When the extreme rainfall events are longer in time, TMPA-RT and CMORPH slightly underestimated LLE events as opposed to Hydro and PERSIANN-GCCS, which tend to overestimate them. Compared with the short-duration events, satellite products performed

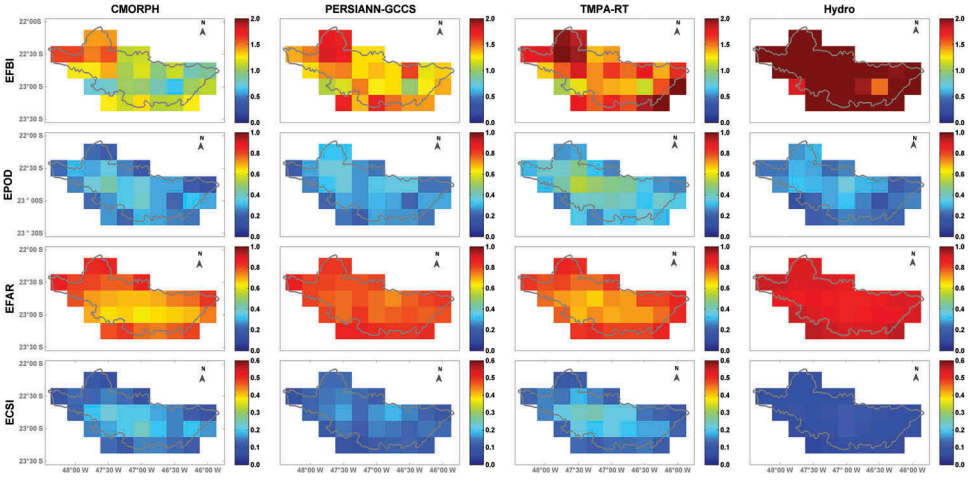

Figure 4. Performance of NRT products in estimating LSE events.

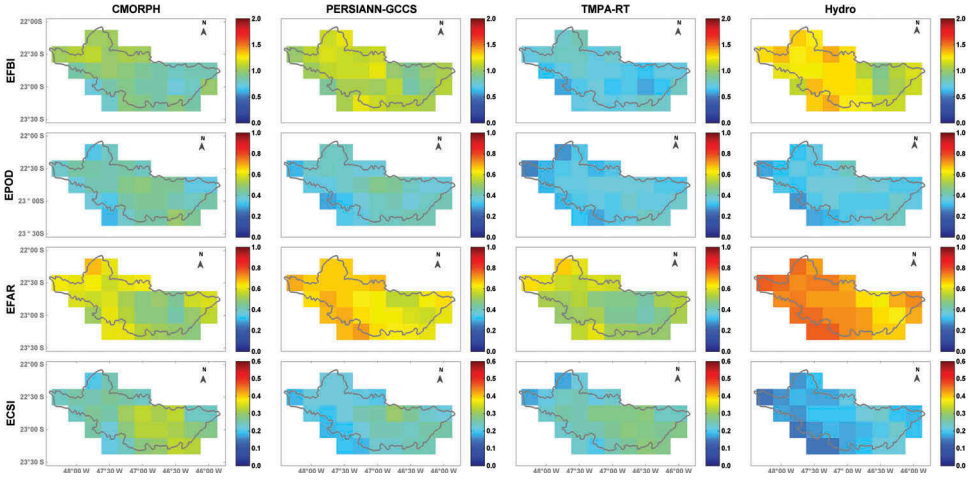

Figure 5. Performance of NRT products in estimating LLE events.

better in detecting LLE events, with higher EPOD detection and a fewer EFAR estimations. CMORPH had a better EPOD score, while TMPA-RT had a better score in false alarm estimations. Overall, CMORPH presented the highest performance for LEE events with a mean ESCI of 0.23, followed by TMPA-RT and PERSIANN-GCCS. Hydro is the product with the lowest performance for LSE.

6.2.3. *Spatially extensive extreme (SEE) events*

Performances for SEE events are presented in Figure 6. The results show the limited capacity of satellite products to detect this type of extreme event. Hydro was highly biased over the whole catchment while PERSIANN-GCCS and TMPA-RT were biased mainly over lower altitude areas. On the other hand, CMORPH was unbiased in lower

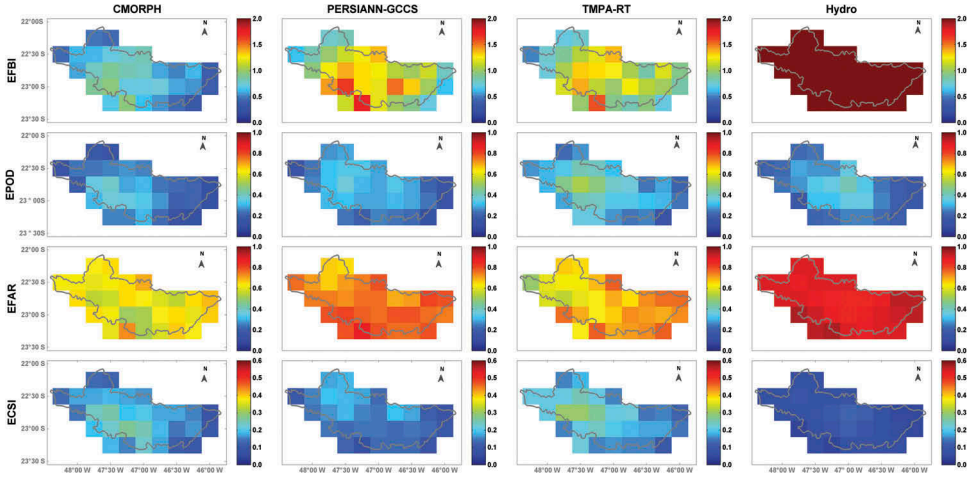

Figure 6. Performance of NRT products in estimating SEE events.

zones, but underestimates over the elevated areas. Regarding the capacity to detect SEE events, TMPA-RT is better, with a high EPOD score over lower zones. CMORPH had the lowest number of false alarm detections with an EFAR value around 0.6. In general, TMPA-RT had the best performance for SEE events with a mean ECSI of 0.2, followed by CMORPH with a mean ECSI of 0.15, PERSIANN-GCCS with a mean ECSI of 0.14, and finally Hydro with ESCI of 0.1.

6.2.4. *Long-lasting and spatially extensive extreme (SLE) events*

Figure 7 shows the performance of satellite products for the SLE events, and one can see the products' higher performance. CMORPH and TMPA-RT were slightly unbiased while Hydro and PERSIANN-GCCS were slightly biased, mainly in low and middle altitude

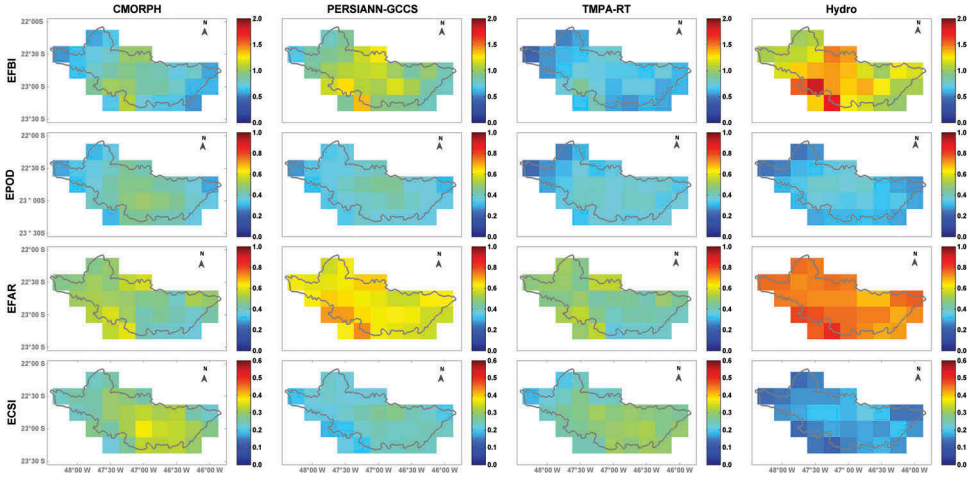

Figure 7. Performance of NRT products in estimating SLE events.

zones. In comparison, CMORPH was slightly better in EPOD and, together with TMPA-RT, showed the lowest false alarm score.

In terms of ECSI, CMORPH had the best performance for detecting SLE events with a mean ECSI value of 0.3 distributed over middle and high altitude zones. In contrast, Hydro was the product with the lowest score with a mean ECSI of 0.15.

6.3. *Event-based performance at different rainfall intensity thresholds*

In order to analyse the influence of the intensity threshold on the evaluation of satellite performance, Figure 8 shows the comparison between the skill scores for each type of event and the rainfall intensity threshold defined as strong, extreme, and most extreme rainfall (above T^{75}, T^{90}, and T^{95}, respectively). Lines show the average values in the whole area, while the shaded regions enveloping them represent the dispersion between the 25th and 75th percentiles. Downward- and upward-pointing triangles are the minimum and maximum score levels for each product.

It can be found that the performance strongly depends on the rainfall intensity level. In all products, the Bias increases as event thresholds increase, especially for Hydro, where the EFBI level in LSE and SEE increases significantly. Short-duration rainfall events were more difficult to estimate than the extensive ones. In the case of EPOD, the product performance marginally decreased for high-intensity events. However, EFAR results had a steadily increased trend as the event threshold increases showing considerable deterioration EFAR scores at higher thresholds. Overall, the capacity of estimating different rainfall events in terms of ECSI showed that long temporal rainfall event score for all products had a steep drop (50% approximately), except TMPA-RT, the score of which also dropped, but just marginally. The ECSI score for short-duration events had

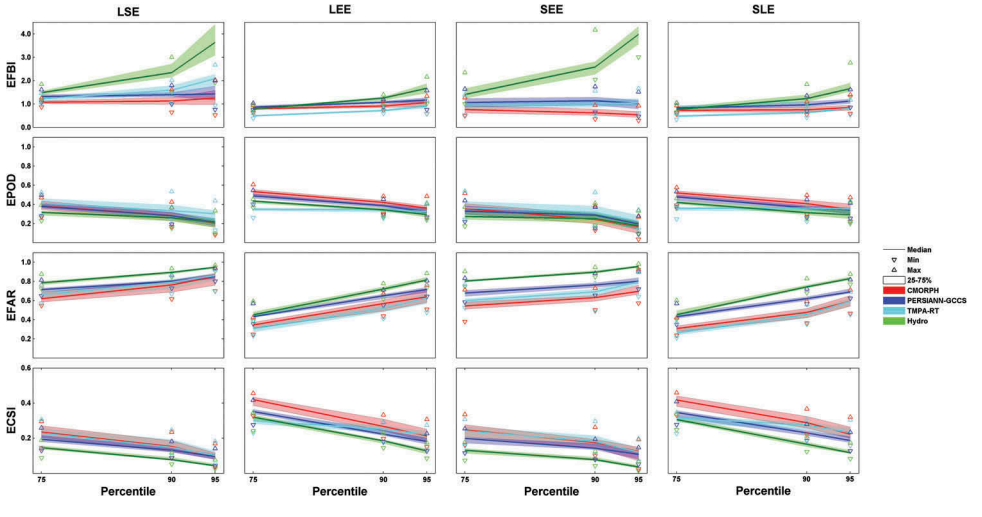

Figure 8. The performance of the four products for EREs of different intensities. Lines are 50% percentiles; shaded ranges – 25% and 75% percentiles. Downward- and upward-pointing triangles are the minimum and maximum score levels for each product.

dropped around 30% for all products, which demonstrates low sensitivity at higher intensities.

7. Conclusions

In this study, we evaluated the performance of four NRT satellite-based products for representing different types of ERE in the subtropical catchment of the Piracicaba, Capivari, and Jundiai rivers in Brazil. CMORPH, PERSIANN-GCCS, TMPA-RT, and Hydro were compared against hourly rain gauge information from AWS during monsoon seasons from 2007 to 2014. The applied methodology identified the spatiotemporal characteristics of extreme rainfall events, classifying them as four EREs according to their magnitude, duration, and spatial extent. We analysed the errors at different rainfall intensities, the performance to detect different extreme events, and the sensitivity of the performance at different thresholds.

We can conclude that all products tend to overestimate rainfall over the study area, specially over high altitude zones. CMORPH had the lowest quantitative error in *r*, RMSE, and Bias at the point-based location. However, TMPA-RT showed lower Bias at high intensities levels. On the other hand, Hydro was the product with the highest error over the whole study area.

The performance of the NRT rainfall products depends on the spatiotemporal characteristics of rainfall events. In general, the short-duration events are more difficult to predict than the long ones. For all ERE types, the study showed that CMORPH and TMPA-RT products exhibited the best performance while PERSIANN-GCCS and Hydro displayed the lowest. TMPA-RT had the best EPOD detections for short temporal events in the same way as CMORPH in spatially extensive events. CMORPH presented the lowest false alarm detections in short-duration events and together with TMPA-RT had the lowest EFAR for spatially extensive events. For ECSI, CMORPH showed the highest performance of all satellite products.

It has been found that the performance of the products is strongly affected by the intensity of rainfall events: the bias increases with intensity. Concerning the capacity to predict different types of events, in most of the rainfall products, the performance of correct estimations marginally decreased, while the frequency of incorrect estimations considerably increased for high-intensity rainfalls. In general, the performance of all products decreased at high rainfall for all types of events.

The results show the importance of taking into account the spatiotemporal characteristics for product verification. Even though the methodology analyses the characteristics of the extreme event using a pixel-based approach, the results show an interesting evaluation of the capabilities of NRT to estimate different EREs. Further research will incorporate new verification methods such as feature-based methods to analyse the spatiotemporal structure of extreme events. These methods can be easily applied to evaluate the capabilities of products at different resolutions without using upscaling techniques, which may contribute to the product error. Another further approach can be the selection of an optimal combination of products. The technology of fuzzy committee models (e.g. Fenicia et al. 2007; Kayastha et al. 2013) could be a possible candidate for this.

Acknowledgments

This work is part of a PhD study of the first author, patially funded by the Colombian Administrative department of Science, Technology and Innovation (COLCIENCIAS), under Grand number 646. The authors would like to acknowledge Ms Maria Clara Fava from the University of São Paulo and Ms Denise Silva and Mr Ricardo Aguilera from Agronomic Intitute CIIAGRO – FUNDAG São Paulo State Government for providing the hourly data from the automatic weather stations and the agencies responsible for satellite database used in this research.

Disclosure statement

No potential conflict of interest was reported by the authors.

Funding

This work is part of a PhD study of the first author, patially funded by the Colombian Administrative department of Science, Technology and Innovation (COLCIENCIAS), under [Grant number 646].

Author contributions

M.L. and G.C. designed the experiments. M.L. extracted and processed the information. M.L. G.C., D.S., and J.D. analysed the information. M.L., G.C., D.S., and J.D. wrote the article.

ORCID

M. Laverde-Barajas http://orcid.org/0000-0002-6901-4019
G.A. Corzo Perez http://orcid.org/0000-0002-2773-7817
J.G. Dalfré Filho http://orcid.org/0000-0001-8105-6177
D.P Solomatine http://orcid.org/0000-0003-2031-9871

References

AghaKouchak, A., A. Behrangi, S. Sorooshian, K. Hsu, and E. Amitai. 2011. "Evaluation of Satellite-Retrieved Extreme Precipitation Rates across the Central United States." *Journal of Geophysical Research: Atmospheres* 116 (D2): D02115. doi:10.1029/2010JD014741.

AghaKouchak, A., and A. Mehran. 2013. "Extended Contingency Table: Performance Metrics for Satellite Observations and Climate Model Simulations." *Water Resources Research* 49 (10): 7144–7149. doi:10.1002/wrcr.20498.

Azarderakhsh, M., W. B. Rossow, F. Papa, H. Norouzi, and R. Khanbilvardi. 2011. "Diagnosing Water Variations within the Amazon Basin Using Satellite Data." *Journal of Geophysical Research: Atmospheres* 116 (D24): D24107. doi:10.1029/2011JD015997.

Boers, N., B. Bookhagen, N. Marwan, and J. Kurths. 2015. "Spatiotemporal Characteristics and Synchronization of Extreme Rainfall in South America with Focus on the Andes Mountain Range." *Climate Dynamics* 46 (1–2): 601–617. doi:10.1007/s00382-015-2601-6.

Boers, N., B. Bookhagen, N. Marwan, J. Kurths, and J. Marengo. 2013. "Complex Networks Identify Spatial Patterns of Extreme Rainfall Events of the South American Monsoon System." *Geophysical Research Letters* 40 (16): 4386–4392. doi:10.1002/grl.50681.

CIIAGRO, Centro Integrado de Informações Agrometeorológicas. 2017. "Rede Meteorológica Automática." Accessed 22 September 2017. http://www.ciiagro.org.br

Dembélé, M., and S. J. Zwart. 2016. "Evaluation and Comparison of Satellite-Based Rainfall Products in Burkina Faso, West Africa." *International Journal of Remote Sensing* 37 (17): 3995–4014. doi:10.1080/01431161.2016.1207258.

Dinku, T., P. Ceccato, E. Grover-Kopec, M. Lemma, S. J. Connor, and C. F. Ropelewski. 2007. "Validation of Satellite Rainfall Products over East Africa's Complex Topography." *International Journal of Remote Sensing* 28 (7): 1503–1526. doi:10.1080/01431160600954688.

Dunkerley, D. 2008. "Rain Event Properties in Nature and in Rainfall Simulation Experiments: A Comparative Review with Recommendations for Increasingly Systematic Study and Reporting." *Hydrological Processes* 22 (22): 4415–4435. doi:10.1002/hyp.7045.

Dunkerley, D. L. 2010. "How Do the Rain Rates of Sub-Event Intervals Such as the Maximum 5- and 15-Min Rates (I5 or I30) Relate to the Properties of the Enclosing Rainfall Event?" *Hydrological Processes* 24 (17): 2425–2439. doi:10.1002/hyp.7650.

Fenicia, F., D. P. Solomatine, H. H. G. Savenije, and P. Matgen. 2007. "Soft Combination of Local Models in a Multi-Objective Framework." *Hydrol Earth Systems Sciences* 11 (6): 1797–1809. doi:10.5194/hess-11-1797-2007.

Gebere, S. B., T. Alamirew, B. J. Merkel, and A. M. Melesse. 2015. "Performance of High Resolution Satellite Rainfall Products over Data Scarce Parts of Eastern Ethiopia." *Remote Sensing* 7 (9): 11639–11663. doi:10.3390/rs70911639.

Gebregiorgis, A. S., and F. Hossain. 2015. "How Well Can We Estimate Error Variance of Satellite Precipitation Data around the World?" *Atmospheric Research* 154: 39–59. doi:10.1016/j.atmosres.2014.11.005.

Guo, H., S. Chen, A. Bao, H. Jujun, A. S. Gebregiorgis, X. Xue, and X. Zhang. 2015. "Inter-Comparison of High-Resolution Satellite Precipitation Products over Central Asia." *Remote Sensing* 7 (6): 7181–7211. doi:10.3390/rs70607181.

Hasan, M. M., A. Sharma, F. Johnson, G. Mariethoz, and A. Seed. 2014. "Correcting Bias in Radar Z–R Relationships Due to Uncertainty in Point Rain Gauge Networks." *Journal of Hydrology* 519: 1668–1676. doi:10.1016/j.jhydrol.2014.09.060.

He, L., X. Ren, Q. Gao, X. Zhao, B. Yao, and Y. Chao. 2017. "The Connected-Component Labeling Problem: A Review of State-Of-The-Art Algorithms." *Pattern Recognition* 70 (Supplement C): 25–43. doi:10.1016/j.patcog.2017.04.018.

Hu, Z., H. Qi, C. Zhang, X. Chen, and L. Qingxiang. 2016. "Evaluation of Reanalysis, Spatially Interpolated and Satellite Remotely Sensed Precipitation Data Sets in Central Asia." *Journal of Geophysical Research: Atmospheres* 121 (10): 2016JD024781. doi:10.1002/2016JD024781.

Huffman, G. J., D. T. Bolvin, E. J. Nelkin, D. B. Wolff, R. F. Adler, G. Guojun, Y. Hong, K. P. Bowman, and E. F. Stocker. 2007. "The TRMM Multisatellite Precipitation Analysis (TMPA): Quasi-Global, Multiyear, Combined-Sensor Precipitation Estimates at Fine Scales." *Journal of Hydrometeorology* 8 (1): 38–55. doi:10.1175/JHM560.1.

Huffman, G. J., R. F. Adler, D. T. Bolvin, and E. J. Nelkin. 2010. "The TRMM Multi-Satellite Precipitation Analysis (TMPA)." In *Satellite Rainfall Applications for Surface Hydrology*, edited by M. Gebremichael and F. Hossain, 3–22. Dordrecht: Springer.doi:10.1007/978-90-481-2915-7_1.

Joyce, R. J., J. E. Janowiak, P. A. Arkin, and P. Xie. 2004. "CMORPH: A Method that Produces Global Precipitation Estimates from Passive Microwave and Infrared Data at High Spatial and Temporal Resolution." *Journal of Hydrometeorology* 5 (3): 487–503. doi:10.1175/1525-7541(2004)005<0487:CAMTPG>2.0.CO;2.

Kayastha, N., J. Ye, F. Fenicia, V. Kuzmin, and D. P. Solomatine. 2013. "Fuzzy Committees of Specialized Rainfall-Runoff Models: Further Enhancements and Tests." *Hydrol Earth Systems Sciences* 17 (11): 4441–4451. doi:10.5194/hess-17-4441-2013.

Kidd, C., A. Becker, G. J. Huffman, C. L. Muller, P. Joe, G. Skofronick-Jackson, and D. B. Kirschbaum. 2016. "So, How Much of the Earth's Surface Is Covered by Rain Gauges?" *Bulletin of the American Meteorological Society* 98 (1): 69–78. doi:10.1175/BAMS-D-14-00283.1.

Kidd, C., V. Levizzani, J. Turk, and R. Ferraro. 2009. "'Satellite Precipitation Measurements for Water Resource Monitoring1'." *JAWRA Journal of the American Water Resources Association* 45 (3): 567–579. doi:10.1111/j.1752-1688.2009.00326.x.

Li, X., Q. Zhang, and C.-Y. Xu. 2014. "Assessing the Performance of Satellite-Based Precipitation Products and Its Dependence on Topography over Poyang Lake Basin." *Theoretical and Applied Climatology* 115 (3–4): 713–729. doi:10.1007/s00704-013-0917-x.

Marra, F., E. Morin, N. Peleg, Y. Mei, and E. N. Anagnostou. 2017. "Intensity–Duration–Frequency Curves from Remote Sensing Rainfall Estimates: Comparing Satellite and Weather Radar over the Eastern Mediterranean." *Hydrol Earth Systems Sciences* 21 (5): 2389–2404. doi:10.5194/hess-21-2389-2017.

Mehran, A., and A. Amir. 2014. "Capabilities of Satellite Precipitation Datasets to Estimate Heavy Precipitation Rates at Different Temporal Accumulations." *Hydrological Processes* 28 (4): 2262–2270. doi:10.1002/hyp.9779.

Mei, Y., E. I. Nikolopoulos, E. N. Anagnostou, and M. Borga. 2015. "Evaluating Satellite Precipitation Error Propagation in Runoff Simulations of Mountainous Basins." *Journal of Hydrometeorology* 17 (5): 1407–1423. doi:10.1175/JHM-D-15-0081.1.

Mei, Y., E. N. Anagnostou, E. I. Nikolopoulos, and M. Borga. 2014. "Error Analysis of Satellite Precipitation Products in Mountainous Basins." *Journal of Hydrometeorology* 15 (5): 1778–1793. doi:10.1175/JHM-D-13-0194.1.

Michaelides, S., V. Levizzani, E. Anagnostou, P. Bauer, T. Kasparis, and J. E. Lane. 2009. "Precipitation: Measurement, Remote Sensing, Climatology and Modeling." *Atmospheric Research* 94(4): 512–533. Precipitation science: measurement, remote sensing, climatology and modellingEGU08 PrecipitationEuropean Geosciences Union General Assembly. doi:10.1016/j.atmosres.2009.08.017.

Moazami, S., S. Golian, M. R. Kavianpour, and Y. Hong. 2013. "Comparison of PERSIANN and V7 TRMM Multi-Satellite Precipitation Analysis (TMPA) Products with Rain Gauge Data over Iran." *International Journal of Remote Sensing* 34 (22): 8156–8171. doi:10.1080/01431161.2013.833360.

NASA. 2000. "TRMM (TMPA-RT) Near Real-time Precipitation L3 3 hour 0.25 degree X 0.25." Accessed 1 May 2016. ftp://disc2.nascom.nasa.gov/data/TRMM/Gridded/3B42RT/

NOAA. 2002a. "CPC Morphing Technique (CMORPH) Global Precipitation Analyses." Accessed 1 May 2016. http://ftp.cpc.ncep.noaa.gov/precip/CMORPH_V1.0/RAW/

NOAA. 2002b. "Operational Hydro-Estimator Satellite Rainfall Estimates." Accessed 1 May 2016. ftp://ftp.star.nesdis.noaa.gov/pub/smcd/emb/f_f/hydroest/world/world/

Pan, M., H. Li, and E. Wood. 2010. "Assessing the Skill of Satellite-Based Precipitation Estimates in Hydrologic Applications." *Water Resources Research* 46 (9): W09535. doi:10.1029/2009WR008290.

Peleg, N., F. Marra, S. Fatichi, A. Paschalis, P. Molnar, and P. Burlando. 2016."Spatial Variability of Extreme Rainfall at Radar Subpixel Scale." *Journal of Hydrology*, May. doi:10.1016/j.jhydrol.2016.05.033.

Peleg, N., M. Ben-Asher, and E. Morin. 2013. "Radar Subpixel-Scale Rainfall Variability and Uncertainty: Lessons Learned from Observations of a Dense Rain-Gauge Network." *Hydrol Earth Systems Sciences* 17 (6): 2195–2208. doi:10.5194/hess-17-2195-2013.

Qiao, L., Y. Hong, S. Chen, C. B. Zou, J. J. Gourley, and B. Yong. 2014. "Performance Assessment of the Successive Version 6 and Version 7 TMPA Products over the Climate-Transitional Zone in the Southern Great Plains, USA." *Journal of Hydrology* 513 (May): 446–456. doi:10.1016/j.jhydrol.2014.03.040.

Ringard, J., M. Becker, F. Seyler, and L. Linguet. 2015. "Temporal and Spatial Assessment of Four Satellite Rainfall Estimates over French Guiana and North Brazil." *Remote Sensing* 7 (12): 16441–16459. doi:10.3390/rs71215831.

Sapiano, M. R. P., and P. A. Arkin. 2009. "An Intercomparison and Validation of High-Resolution Satellite Precipitation Estimates with 3-Hourly Gauge Data." *Journal of Hydrometeorology* 10 (1): 149–166. doi:10.1175/2008JHM1052.1.

Scofield, R. A., and R. J. Kuligowski. 2003. "Status and Outlook of Operational Satellite Precipitation Algorithms for Extreme-Precipitation Events." *Weather and Forecasting* 18 (6): 1037–1051. doi:10.1175/1520-0434(2003)018<1037:SAOOOS>2.0.CO;2.

Sorooshian, S., K.-L. Hsu, X. Gao, H. V. Gupta, B. Imam, and D. Braithwaite. 2000. "Evaluation of PERSIANN System Satellite-Based Estimates of Tropical Rainfall." *Bulletin of the American*

Meteorological Society 81 (9): 2035–2046. doi:10.1175/1520-0477(2000)081<2035:EOPSSE>2.3.CO;2.

Sprissler, T. 2011. *Flood Risk Brazil: Prevention, Adaptation and Insurance*. Switzerland. http://media.swissre.com/documents/Staying_on_top_of_flood_risk_in_Brazil.pdf

Szeliski, R. 2010. *Computer Vision: Algorithms and Applications*. Springer Science & Business Media. London: Springer. doi: 10.1007/978-1-84882-935-0.

Thiemig, V., R. Rojas, M. Zambrano-Bigiarini, V. Levizzani, and A. De Roo. 2012. "Validation of Satellite-Based Precipitation Products over Sparsely Gauged African River Basins." *Journal of Hydrometeorology* 13 (6): 1760–1783. doi:10.1175/JHM-D-12-032.1.

UC Irvine. 2003. "Precipitation Estimation from Remotely Sensed Information using Artificial Neural Networks." Accessed 1 May 2016. ftp://persiann.eng.uci.edu/pub/GCCS/

Vicente, G. A., R. A. Scofield, and W. Paul Menzel. 1998. "The Operational GOES Infrared Rainfall Estimation Technique." *Bulletin of the American Meteorological Society* 79 (9): 1883–1898. doi:10.1175/1520-0477(1998)079<1883:TOGIRE>2.0.CO;2.

Villarini, G., F. Serinaldi, and W. F. Krajewski. 2008. "Modeling Radar-Rainfall Estimation Uncertainties Using Parametric and Non-Parametric Approaches." *Advances in Water Resources* 31 (12): 1674–1686. doi:10.1016/j.advwatres.2008.08.002.

Wackernagel, H. 2003. *Multivariate Geostatistics*. 3rd ed. Berlin: Springer. doi: 10.1007/978-3-662-05294-5

Wilks, D. S. 2011. *Statistical Methods in the Atmospheric Sciences*. Academic Press. ISBN: 9780123850232. https://www.elsevier.com/books/statistical-methods-in-the-atmospheric-sciences/wilks/978-0-12-385022-5

Yong, B., D. Liu, J. J. Gourley, Y. Tian, G. J. Huffman, L. Ren, and Y. Hong. 2014. "Global View Of Real-Time Trmm Multisatellite Precipitation Analysis: Implications For Its Successor Global Precipitation Measurement Mission." *Bulletin of the American Meteorological Society* 96 (2): 283–296. doi:10.1175/BAMS-D-14-00017.1.

Yong, B., L. Ren, Y. Hong, J. Wang, J. J. Gourley, S. Jiang, X. Chen, and W. Wang. 2010. "Hydrologic Evaluation of Multisatellite Precipitation Analysis Standard Precipitation Products in Basins beyond Its Inclined Latitude Band: A Case Study in Laohahe Basin, China." *Water Resources Research* 46 (7). doi:10.1029/2009WR008965.

Yong, B., Y. Hong, -L.-L. Ren, J. J. Gourley, G. J. Huffman, X. Chen, W. Wang, and S. I. Khan. 2012. "Assessment of Evolving TRMM-Based Multisatellite Real-Time Precipitation Estimation Methods and Their Impacts on Hydrologic Prediction in a High Latitude Basin." *Journal of Geophysical Research: Atmospheres* 117 (D9): D09108. doi:10.1029/2011JD017069.